Semi-local scaling and turbulence modulation in variable property turbulent channel flows

Ashish Patel,[a)] Jurriaan W. R. Peeters, Bendiks J. Boersma, and Rene Pecnik[b)]

Process and Energy Department, Delft University of Technology, Leeghwaterstraat 39, 2628 CB Delft, The Netherlands

We theoretically and numerically investigate the effect of temperature dependent density and viscosity on turbulence in channel flows. First, a mathematical framework is developed to support the validity of the semi-local scaling as proposed based on heuristic arguments by Huang, Coleman, and Bradshaw ["Compressible turbulent channel flows: DNS results and modelling," J. Fluid Mech. **305**, 185–218 (1995)]. Second, direct numerical simulations (DNS) of turbulent channel flows with different constitutive relations for density and viscosity are performed to assess and validate the semi-local scaling for turbulent statistics. The DNS database is obtained by solving the low-Mach number approximation of the Navier-Stokes equation. Finally, we quantify the modulation of turbulence due to changes in fluid properties. In the simulations, the fluid is internally heated and the temperature at both channel walls is fixed, such that the friction Reynolds number based on wall quantities is $Re_\tau = 395$ for all cases investigated. We show that for a case with variable density ρ and viscosity μ, but constant semi-local Reynolds number $Re_\tau^* \equiv \sqrt{(\overline{\rho}/\rho_w)}/(\overline{\mu}/\mu_w)Re_\tau$ (where bar and subscript w, denote Reynolds averaging and averaged wall quantity, respectively), across the whole channel height, the turbulent statistics exhibit quasi-similarity with constant property turbulent flows. For cases where $Re_\tau^* \neq Re_\tau$ across the channel, we found that quasi-similarity is maintained for cases with similar Re_τ^* distributions, even if their individual mean density and viscosity profiles substantially differ. With a decrease of Re_τ^* towards the channel center ($Re_\tau^* < Re_\tau$), we show that the anisotropy increases and the pre-multiplied stream-wise spectra reveal that this increase is associated with strengthening of the large scale streaks in the buffer layer. The opposite effect is observed when Re_τ^* increases towards the channel center. The present results provide an effective framework for categorizing turbulence modulation in wall-bounded flows with variable property effects, and can be applied to any Newtonian fluid that is heated or cooled. © *2015 AIP Publishing LLC.* [http://dx.doi.org/10.1063/1.4929813]

I. INTRODUCTION

Heat transfer plays an important role in many engineering applications and affects many sectors of modern economy. In some of the applications, the effects of temperature dependent thermo-physical properties are strong and the traditional approach of treating temperature as a passive scalar no longer holds. The strong coupling between energy and momentum alters the conventional behaviour of turbulence and conventional scaling laws for constant property flows fail and cannot be applied. Classical scaling laws for flows with constant thermo-physical properties have been investigated in great detail by Moser, Kim, and Mansour,[2] Hoyas and Jiménez,[3] Bernardini, Pirozzoli, and Orlandi,[4] and references therein. While the classical scaling is able to provide an approximate collapse of Reynolds

---

a)Electronic mail: a.patel@tudelft.nl
b)Electronic mail: r.pecnik@tudelft.nl

27, 095101-1

stresses in the inner-layer, there is no universal scaling with respect to Reynolds number.[3,5] The peak amplitude of stream-wise and span-wise fluctuations increases logarithmically with Re_τ, while wall-normal fluctuations increase sub-logarithmically.[4] The influence of large-scale outer-layer motions on the near-wall cycle increases with Reynolds number.[5–7] There has been considerable progress in understanding how turbulence intensities depend on the Reynolds number and predictive models for estimating them have been proposed by Marusic, Mathis, and Hutchins.[7,8]

Studies on variable property wall turbulence have been performed mostly for high Mach number flows. Smits[9] investigated supersonic turbulent boundary layer flows and commented that a single Reynolds number cannot be used to characterize the state of the boundary layer due to variations in properties. Coleman, Kim, and Moser[10] investigated a supersonic channel flow using DNS with cold isothermal walls and concluded that only mean property variations, but not thermodynamic fluctuations, are important at supersonic Mach numbers. They observed that the property variations lead to an enhanced streak coherence (longer streaks) when compared to incompressible cases. A streak-elongation was also reported for supersonic turbulent boundary layers with cooled walls by Duan, Beekman, and Martin[11] and Lagha *et al.*,[12] while shorter streaks were observed for heated walls by Duan, Beekman, and Martin.[11] These streak modifications were quantified in terms of wall based viscous units. Huang, Coleman, and Bradshaw[1] proposed a semi-local scaling based on wall shear stress and local properties to collapse the turbulent statistics in the near-wall region. The semi-local scaling was used by Coleman, Kim, and Moser[10] to compare their compressible results with incompressible data and a good qualitative agreement was obtained. Morinishi, Tamano, and Nakabayashi[13] performed DNS of compressible turbulent channel flows between adiabatic and isothermal walls at a relatively low-Reynolds number of $Re_\tau = 150$. They showed that the near-wall velocity streaks for compressible turbulent flows do not become more coherent and are independent of thermal wall boundary conditions if semi-local units are used to compare with incompressible flows. Nicoud and Poinsot[14] performed a DNS (using the low Mach number approximation of the Navier–Stokes equations) of a variable property channel flow with both walls at different but constant temperatures. The semi-local scaling was used to highlight differences in span-wise and wall-normal peak turbulent intensities when compared with the isothermal flow. Foysi, Sarkar, and Friedrich[15] further analysed the applicability of the semi-local scaling for a turbulent supersonic channel flow with isothermal walls. They observed that in the inner-layer the stream-wise Reynolds stress component increased, while the span-wise and the wall-normal components decreased when compared with the constant property case. This increase in anisotropy was attributed to the non-local dependence of the pressure strain on density, where a decrease of density causes the pressure-strain correlation to decrease. They concluded that the semi-local scaling gives a better performance as compared to the classical wall scaling, but the improvement is only partial, because of the non-local dependence of pressure on density.

In the present work, we attempt to clarify and quantify in detail the effect of variable density and viscosity on near-wall turbulence modification and scaling of turbulent statistics. We provide a mathematical basis for the use of semi-local scaling, which was proposed by Huang, Coleman, and Bradshaw.[1] A fully developed channel flow, driven by a constant stream-wise pressure gradient, is studied under the low Mach number approximation of the Navier-Stokes equations without the effect of buoyancy. The fluid is heated by a volumetric heat source, as in the passive scalar simulations of Kim and Moin.[16] Furthermore, the computational setup can be considered qualitatively similar to that of Huang, Coleman, and Bradshaw,[1] Coleman, Kim, and Moser,[10] Foysi, Sarkar, and Friedrich,[15] because density and viscosity are coupled to the temperature and the volumetric heat source mimics the viscous heating for supersonic flows. However, the volumetric heating is set constant (in contrast to viscous heating) and the acoustic effects are not taken into account in the present simulations. Based on previous experimental and numerical studies,[10,12,17–21] it is known that for supersonic flows with moderate Mach numbers ($Ma < 5$), the direct effects of compressibility on wall turbulence are small and any differences from incompressible turbulence can be accounted for by mean variations of fluid properties. In the near-wall region of a supersonic flow, most of the near-wall density and temperature fluctuations are the result of solenoidal "passive mixing" by turbulence, and density fluctuations show little correlation with pressure fluctuations.[10,17] In that respect, studying the influence of property gradients without intrinsic compressibility effects is in

line with previous studies on supersonic wall-bounded flows. Therefore, even though the database in present work is obtained using a low-Mach number approximation of the Navier-Stokes equation, the results are of relevance to flows in the supersonic regime. Seven DNS cases with different combinations of density and viscosity as a function of temperature are simulated, and selected cases are compared to each other.

II. METHODOLOGY

A. Governing equations and computational approach

The low Mach number approximation of the Navier-Stokes equations in Cartesian co-ordinates is solved to simulate the turbulent flow in a channel. In the low Mach number limit, acoustic wave propagation is ignored and the pressure field is decomposed into a thermodynamic $P_0(t)$ and a hydrodynamic component $p(x_i, t)$.[22,23] Furthermore, for a calorifically perfect fluid in a closed system with zero net heat flux, it can be shown that P_0 is independent of time.[24] The density and transport properties can then be evaluated independently of the hydrodynamic pressure variations ($p \ll P_0$) as a function of temperature alone. Under these assumptions, the governing equations for mass, momentum, and energy can be expressed in non-dimensional form, without effects of buoyancy, as

$$\partial_t \rho + \partial_{x_j}(\rho u_j) = 0, \tag{1}$$

$$\partial_t(\rho u_i) + \partial_{x_j}(\rho u_i u_j) = -\partial_{x_i} p + \frac{1}{Re_\tau} \partial_{x_j}\left(2\mu S_{ij}\right), \tag{2}$$

$$\partial_t(\rho H) + \partial_{x_j}(\rho u_j H) = \frac{1}{Re_\tau Pr_w} \partial_{x_j}(\lambda \partial_{x_j} T) + \frac{\phi}{Re_\tau Pr_w}, \tag{3}$$

with the strain rate tensor $S_{ij} = \frac{1}{2}\left(\partial_{x_j} u_i + \partial_{x_i} u_j\right) - \frac{1}{3} \partial_{x_k} u_k \delta_{ij}$ and δ_{ij} the Kronecker delta. The equations are written in non-dimensional form by using the following non-dimensional variables:

$$x_i = \frac{x_i^0}{h^0}, \quad t = \frac{t^0}{h^0/u_\tau^0}, \quad u_i = \frac{u_i^0}{u_\tau^0}, \quad p = \frac{p^0}{\rho_w^0 u_\tau^{0^2}}, \quad T = \frac{T^0}{T_w^0},$$

$$H = \frac{H^0}{c_{pw}^0 T_w^0}, \quad \rho = \frac{\rho^0}{\rho_w^0}, \quad \lambda = \frac{\lambda^0}{\lambda_w^0}, \quad c_p = \frac{c_p^0}{c_{pw}^0}, \quad \mu = \frac{\mu^0}{\mu_w^0}, \tag{4}$$

where $x_i, t, u_i, p, T, H, \rho, \lambda, c_p,$ and μ are the spatial co-ordinates, time, velocity, pressure, temperature, enthalpy, density, thermal conductivity, isobaric heat capacity, and dynamic viscosity, respectively, with the superscript 0 indicating the dimensional quantities and subscript w the averaged wall values. $u_\tau^0 = \sqrt{\tau_w^0/\rho_w^0}$ is the friction velocity based on wall values and h^0 is the half channel height. The Reynolds number and Prandtl number are $Re_\tau = \rho_w^0 u_\tau^0 h^0/\mu_w^0$ and $Pr_w = \mu_w^0 c_{pw}^0/\lambda_w^0$, respectively. In order to achieve variations in temperature T, and consequently in density ρ and viscosity μ, the flow is uniformly heated with a volumetric heat source ϕ, while the temperature at both channel walls is kept constant. In this manner, the symmetry of the mean flow is maintained and the Reynolds number Re_τ is constant with respect to property variations. This forms the basis for an ideal setup to study turbulence modification due to variable properties, and to compare scaling laws with isothermal flows, as compared to a case where the bottom and top walls are at different temperatures and therefore at different Reynolds numbers.[14,25]

The co-ordinates x, y, z represent the stream-wise, the wall-normal, and the span-wise directions, respectively; the corresponding velocity vectors are represented as u, v, w. The mean statistics are obtained by averaging with respect to time and in homogeneous directions (x and z) using Reynolds and Favre averaging. For a generic variable γ, the Reynolds averaged mean $\overline{\gamma}$ and its fluctuation γ' are defined as $\gamma = \overline{\gamma} + \gamma'$, with $\overline{\gamma'} = 0$. The Favre averaged mean $\tilde{\gamma}$ and its fluctuation γ'' are defined as $\gamma = \tilde{\gamma} + \gamma''$, with $\tilde{\gamma} = \overline{\rho\gamma}/\overline{\rho}$.

A sixth order staggered compact finite difference scheme[26,27] is used to discretize the spatial derivatives in wall-normal direction. In homogeneous directions, the Fourier expansion with periodic boundary conditions is used and the advection term is discretized with a skew-symmetric

formulation of Morinishi.[28] The equations are integrated in time using the second order Adams-Bashforth method. The pressure correction scheme is based on the projection method.[29] The validation of the numerical approach is discussed in Appendix A.

B. Semi-local scaling

Wall scaling for constant property flows utilizes $u_\tau = \sqrt{\tau_w/\rho_w}$ as the velocity scale, and $\delta_v = \mu_w/\rho_w u_\tau$ as the viscous length scale to characterize the inner-layer. The corresponding dimensionless wall co-ordinate is then $y^+ = y/\delta_v$. Semi-local scaling as proposed by Huang, Coleman, and Bradshaw[1] for variable property flows utilizes local properties for the velocity and viscous length scale, such that $u_\tau^* = \sqrt{\tau_w/\overline{\rho}}$ and $\delta_v^* = \overline{\mu}/\overline{\rho} u_\tau^*$, respectively. This leads to the semi-locally scaled wall distance $y^* = y/\delta_v*$ and the corresponding semi-local Reynolds number $Re_\tau^* = h/\delta_v^*$.

For constant property wall-bounded turbulent flows in a given geometry, turbulent statistics are a unique function of wall-normal distance y/h and friction Reynolds number Re_τ, such that $\overline{u_i'u_j'}/u_\tau^2 = f(y/h, Re_\tau)$, where f is a generalized function and not known *a priori*. By applying the classical wall scaling in the inner-layer, the expression for the Reynolds stresses can be reduced to $\overline{u_i'u_j'}/u_\tau^2 \approx f(y^+)$. However, it is known that no universal scaling with respect to Reynolds number exists.[3,5] The peak amplitude of stream-wise and span-wise fluctuations increases logarithmically with Re_τ, while wall-normal fluctuations increase sub-logarithmically,[4] such that it is more appropriate to write the Reynolds stresses as

$$\overline{u_i'u_j'}/u_\tau^2 = f(y^+, Re_\tau). \tag{5}$$

For variable property wall-bounded turbulent flows, turbulent statistics for a given flow geometry not only depend on y/h and Re_τ, but also on the profile of density and viscosity. For moderate density and viscosity gradients, the property fluctuations are small and Morkovin's hypothesis holds, i.e., only mean property variations, but not thermodynamic fluctuations are important in turbulence dynamics.[10] The expression for the Reynolds stresses can then be written as

$$\overline{\rho u_i''u_j''}/\tau_w \approx f(y/h, Re_\tau, \overline{\rho}_p, \overline{\mu}_p). \tag{6}$$

Note, in the above equation $\overline{\rho}_p$ and $\overline{\mu}_p$ are the normalized mean profiles of density and viscosity over the complete channel cross-section. The semi-local scaling proposed by Huang, Coleman, and Bradshaw[1] has been used in the past to account for mean property variations in the near-wall scaling of turbulent statistics for compressible flows when compared with isothermal cases. In the present work, we investigate if the semi-local scaling can be used as an universal near-wall co-ordinate for flows with variable property effects. In other words, we assess if

$$\overline{\rho u_i''u_j''}/\tau_w \approx f(y/h, Re_\tau^*) \approx f(y^*, Re_\tau^*) \tag{7}$$

holds. Equation (7) implies that Re_τ^* is sufficient to characterize near-wall turbulence dynamics. The validation of the above hypothesis will provide a strong support for the semi-local scaling as turbulent statistics at a given wall-normal position will depend only on the Re_τ^* profile, thus providing a framework similar to constant property turbulence, wherein the dependence is only on Re_τ.

C. Mathematical support for the semi-local scaling

In this section, we develop a mathematical foundation for the semi-local scaling that was suggested by Huang, Coleman, and Bradshaw[1] using heuristic arguments. First, we propose to re-scale the Navier-Stokes equations using local quantities defined as

$$\hat{x}_i = \left(\frac{x_i}{h}\right), \quad \hat{t} = \frac{t}{h/u_\tau^*} = \left(\frac{t}{h/u_\tau}\right)\sqrt{\frac{\rho_w}{\overline{\rho}}}, \quad \hat{u}_i = \frac{u_i}{u_\tau^*} = \left(\frac{u_i}{u_\tau}\right)\sqrt{\frac{\overline{\rho}}{\rho_w}}, \quad \hat{p} = \frac{p}{\overline{\rho}u_\tau^{*2}} = \left(\frac{p}{\rho_w u_\tau^2}\right),$$
$$\tag{8}$$

$$\hat{\rho} = \frac{\rho}{\overline{\rho}} = \left(\frac{\rho}{\rho_w}\right)\frac{\rho_w}{\overline{\rho}} = 1 + \frac{\rho'}{\overline{\rho}}, \quad \hat{\mu} = \frac{\mu}{\overline{\mu}} = \left(\frac{\mu}{\mu_w}\right)\frac{\mu_w}{\overline{\mu}} = 1 + \frac{\mu'}{\overline{\mu}}, \tag{9}$$

where $\overline{\rho}$, $\overline{\mu}$, and u_τ^* are time—and homogeneous direction averaged local values of density, viscosity, and semi-local friction velocity, respectively. The terms within brackets indicate the standard normalization used in Equation (4). Using Equations (8) and (9), the re-scaled mass and momentum equations can be written as

$$\partial_{\hat{t}}\hat{\rho} + \partial_{\hat{x}_j}(\hat{\rho}\hat{u}_j) + \frac{\hat{\rho}\hat{v}}{2}\left(\frac{\rho_w}{\overline{\rho}}\right)\partial_{\hat{y}}\left(\frac{\overline{\rho}}{\rho_w}\right) = 0, \tag{10}$$

$$\partial_{\hat{t}}(\hat{\rho}\hat{u}_i) + \partial_{\hat{x}_j}(\hat{\rho}\hat{u}_i\hat{u}_j) = -\partial_{\hat{x}_i}\hat{p} + \partial_{\hat{x}_j}\left[\frac{\hat{\mu}}{Re_\tau^*}\sqrt{\frac{\overline{\rho}}{\rho_w}}\left(\partial_{\hat{x}_j}\left(\hat{u}_i\sqrt{\frac{\rho_w}{\overline{\rho}}}\right) + \partial_{\hat{x}_i}\left(\hat{u}_j\sqrt{\frac{\rho_w}{\overline{\rho}}}\right)\right.\right.$$
$$\left.\left. - \frac{2\delta_{ij}}{3}\partial_{\hat{x}_k}\left(\hat{u}_k\sqrt{\frac{\rho_w}{\overline{\rho}}}\right)\right)\right]. \tag{11}$$

Next, Equations (10) and (11) are used to derive the conservation equations for the mean and the fluctuating component of $\hat{u}_i$. But before doing so, we first discuss the influence of density fluctuations on turbulent statistics by highlighting the relation between Reynolds and Favre decomposition for a generic quantity γ as

$$\overline{\gamma} = \tilde{\gamma} - \frac{\overline{\rho'\gamma'}}{\overline{\rho}}, \tag{12}$$

$$\gamma' = \gamma'' + \frac{\overline{\rho'\gamma'}}{\overline{\rho}}. \tag{13}$$

From Morkovin's hypothesis, it is known that the direct effects of density fluctuations on turbulence are small if the root-mean-square density fluctuation is small compared with the absolute density,[30] i.e., $\sqrt{\overline{\rho'^2}}/\overline{\rho} \ll 1$. Note that Morkovin's hypothesis does not include the effect of viscosity fluctuations and the effects of spatial gradients of mean density.[30] Coleman, Kim, and Moser[10] investigated a supersonic channel flow using DNS with spatial gradients of properties and concluded that only mean property variations, but not thermodynamic fluctuations, govern the turbulence structure. They argued that this fact reinforces Morkovin's hypothesis, as thermodynamic fluctuations have a minor role on the turbulence structure. Therefore, under the validity of Morkovin's hypothesis ($\sqrt{\overline{\rho'^2}}/\overline{\rho} \ll 1$), any turbulent statistics resulting from density fluctuations should be insignificant in comparison to those obtained using mean density. This implies that the second term on the right hand side of Equations (12) and (13) is insignificant, we assess this using the DNS data in Section IV A. The semi-locally scaled velocity components can then be related to the classically scaled velocity components as

$$\frac{\overline{u}}{u_\tau} = \overline{\hat{u}}\sqrt{\frac{\rho_w}{\overline{\rho}}} \approx \frac{\tilde{u}}{u_\tau}, \quad \frac{\overline{v}}{u_\tau} = \overline{\hat{v}}\sqrt{\frac{\rho_w}{\overline{\rho}}} \approx \frac{\tilde{v}}{u_\tau} = 0, \quad \frac{\overline{w}}{u_\tau} = \overline{\hat{w}}\sqrt{\frac{\rho_w}{\overline{\rho}}} \approx \frac{\tilde{w}}{u_\tau} = 0,$$
$$\frac{u'}{u_\tau} = \hat{u}'\sqrt{\frac{\rho_w}{\overline{\rho}}} \approx \frac{u''}{u_\tau}, \quad \frac{v'}{u_\tau} = \hat{v}'\sqrt{\frac{\rho_w}{\overline{\rho}}} \approx \frac{v''}{u_\tau}, \quad \frac{w'}{u_\tau} = \hat{w}'\sqrt{\frac{\rho_w}{\overline{\rho}}} \approx \frac{w''}{u_\tau}. \tag{14}$$

Note that for a fully developed turbulent channel flow, $\tilde{v} = \tilde{w} = 0$. Next, the Reynolds decomposition of density and viscosity can be written using Equation (9) as

$$\overline{\hat{\rho}} = 1, \quad \hat{\rho}' = \frac{\rho'}{\overline{\rho}}, \quad \overline{\hat{\mu}} = 1, \quad \hat{\mu}' = \frac{\mu'}{\overline{\mu}}. \tag{15}$$

Assuming relatively small density and viscosity fluctuations ($\hat{\rho}' = \rho'/\overline{\rho} \ll 1$ and $\hat{\mu}' = \mu'/\overline{\mu} \ll 1$), the Reynolds-averaged continuity and momentum equations for a fully developed flow with $\overline{\hat{v}} = \overline{\hat{w}} \approx 0$ are simplified to

$$\partial_{\hat{x}_j}(\overline{\hat{u}_j}) \approx 0, \tag{16}$$

$$\partial_{\hat{y}}(\overline{\hat{u}_i'\hat{v}'}) \approx -\partial_{\hat{x}_i}\overline{\hat{p}} + \partial_{\hat{y}}\left[\frac{1}{Re_\tau^*}\sqrt{\frac{\overline{\rho}}{\rho_w}}\partial_{\hat{y}}\left(\overline{\hat{u}_i}\sqrt{\frac{\rho_w}{\overline{\rho}}}\right)\right]. \tag{17}$$

Substituting Equation (14) back into Equation (17), we can write the mean stream-wise momentum equation as

$$\partial_y \left(\frac{\overline{\rho u'' v''}}{\tau_w} \right) \approx -\partial_x \left(\frac{\overline{p}}{\tau_w} \right) + \partial_y \left[\frac{1}{Re_\tau^*} \sqrt{\frac{\overline{\rho}}{\rho_w}} \partial_y \left(\frac{\overline{u}}{u_\tau} \right) \right], \tag{18}$$

where $\overline{\hat{u}' \hat{v}'} = \overline{\rho u' v'}/\tau_w \approx \overline{\rho u'' v''}/\tau_w$ based on Morkovin's hypothesis. Note that the above equation could have been obtained also using Reynolds/Favre averaging of the stream-wise momentum equation given by Equation (2), without making any assumption on density fluctuations and only neglecting the viscosity fluctuations. However, this rescaling approach becomes more convenient when analysing the fluctuation equations as done later.

The term $\sqrt{\overline{\rho}/\rho_w} \, \partial(\overline{u}/u_\tau)$ in Equation (18) can be expressed as the van Driest transformed velocity with

$$\partial \overline{u}^{vd} = \sqrt{\frac{\overline{\rho}}{\rho_w}} \, \partial \left(\frac{\overline{u}}{u_\tau} \right). \tag{19}$$

Thus, the turbulent shear stress and the mean velocity profile are related through

$$\partial_y \left(\frac{\overline{\rho u'' v''}}{\tau_w} \right) \approx -\partial_x \left(\frac{\overline{p}}{\tau_w} \right) + \partial_y \left(\frac{1}{Re_\tau^*} \partial_y \overline{u}^{vd} \right). \tag{20}$$

The only governing parameter in this relation is the semi-local scaling parameter Re_τ^*. In other words, flows with similar Re_τ^* profiles will result in similar van Driest transformed velocity and turbulent shear stress profiles. Similarly, the mean wall-normal momentum equation gives the relation between pressure and wall-normal Reynolds stress as $\overline{\rho v'' v''} \approx -\overline{p} + constant$.

The conservation equations for the fluctuating velocity components are derived next to relate second order turbulent statistics with the van Driest velocity and Re_τ^* profiles. Again using similar hypotheses as those for deriving (16) and (17), we obtain the continuity and momentum equations for $\hat{u}_i'$ as

$$\partial_{\hat{x}_j}(\hat{u}_j') + \frac{\hat{v}'}{2} \left(\frac{\rho_w}{\overline{\rho}} \right) \partial_{\hat{y}} \left(\frac{\overline{\rho}}{\rho_w} \right) \approx 0, \tag{21}$$

$$\partial_{\hat{t}}(\hat{u}_i') + \partial_{\hat{x}_j}(\hat{u}_i' \hat{u}_j') + \hat{v}' \partial_{\hat{y}}(\overline{u}^{vd}) \delta_{i1} + \overline{\hat{u}}_j \partial_{\hat{x}_j}(\hat{u}_i') \approx$$
$$-\partial_{\hat{x}_i} \hat{p}' + \partial_{\hat{x}_j}(\overline{\hat{u}_i' \hat{u}_j'}) + \partial_{\hat{x}_j} \left[\frac{1}{Re_\tau^*} \left(2\hat{S}_{ij}' - \hat{D}_{ij} \right) \right], \tag{22}$$

with $\quad \hat{S}_{ij}' = \frac{1}{2} \left(\partial_{\hat{x}_j} \hat{u}_i' + \partial_{\hat{x}_i} \hat{u}_j' \right) - \frac{1}{3} \partial_{\hat{x}_k} \hat{u}_k' \delta_{ij} \quad$ and $\quad \hat{D}_{ij} = \frac{\hat{u}_i'}{2} \left(\frac{\rho_w}{\overline{\rho}} \right) \partial_{\hat{x}_j} \left(\frac{\overline{\rho}}{\rho_w} \right) + \frac{\hat{u}_j'}{2} \left(\frac{\rho_w}{\overline{\rho}} \right) \partial_{\hat{x}_i} \left(\frac{\overline{\rho}}{\rho_w} \right)$ $- \delta_{ij} \frac{\hat{v}'}{3} \left(\frac{\rho_w}{\overline{\rho}} \right) \partial_{\hat{y}} \left(\frac{\overline{\rho}}{\rho_w} \right)$. For a detailed derivation see Appendix B.

This relation can further be used to derive the transport equations for the second order turbulent statistics. Thus, analysing Equation (22) can shed light on the scaling properties of Reynolds stresses, which are not evident from the averaged momentum equations. If Equation (22) is compared with the analogous equation for constant property turbulent flows, three differences can be seen: (1) the third term (production term in the transport equations for the second order turbulent statistics) is governed by the gradient of the van Driest velocity $\overline{u}^{vd}$ instead of $\overline{u}/u_\tau$ as in constant property flows, (2) instead of Re_τ the semi-local Reynolds number Re_τ^* governs the scaling of the viscous term (turbulent dissipation) within the first spatial derivative, and (3) an additional term $\hat{D}_{ij}$ appears that is related to the wall-normal gradient of mean density. Scaling arguments can be used to estimate the ratio of $\hat{S}_{ij}'$ and $\hat{D}_{ij}$. Following Tennekes and Lumley[31] with Λ as the Taylor length scale, these terms can be estimated as $\hat{S}_{ij}' \approx O(\overline{u}/\Lambda)$ and $\hat{D}_{ij} \approx O(\overline{u}/h)$. The ratio is then $\hat{S}_{ij}'/D_{ij} \approx O(h/\Lambda)$, which is far larger than unity for highly turbulent flows, and thus $\hat{D}_{ij}$ plays a minor role on the evolution of turbulent fluctuations. Now, it can be seen that also for Equation (22) the governing parameter is Re_τ^* (in Equation (20) we showed that $\overline{u}^{vd}$ is governed by Re_τ^*) and therefore it can be hypothesized that the second order turbulent statistics also depend on the Re_τ^* profile

only. This allows several conclusions. For example, given a turbulent flow with variable mean density and viscosity, such that Re_τ^* is constant, the van Driest velocity profile $\overline{u}^{vd}$ and the second order turbulent statistics $\widehat{u_i'}\widehat{u_j'} \approx \overline{\rho u_i'' u_j''}/\tau_w$ will overlap with the mean velocity $\overline{u}/u_\tau$ and turbulent statistics $\overline{u_i' u_j'}/u_\tau^2$ from a constant property turbulent flow. Furthermore, similar turbulent statistics and van Driest velocity profiles will be obtained for cases with similar Re_τ^* profiles, even if their density and viscosity profiles substantially differ. Or more general, turbulent flows with similar Re_τ^* profiles will give similar turbulent statistics, provided Morkovin's hypotheses and $\hat{\mu}' \ll 1$ are not invalidated. This hypothesis will be tested by means of numerical experiments outlined in Sec. III.

III. NUMERICAL EXPERIMENTS

Seven cases have been simulated and are summarised in Tables I and II. The DNS database is obtained by solving the governing equations given in Section II A and therefore is not compromised with the assumptions made in Sections II B and II C with respect to density and viscosity fluctuations. The first case corresponds to an isothermal flow, while the remaining six cases are flows with variable density ρ and viscosity μ. The relations for ρ and μ as a function of temperature T are outlined in Table I. Note, that since ρ and μ only depend on T in the present work, the relations for ρ/ρ_w and μ/μ_w on T are the same as for ρ and μ. The h^* values at the channel center are given in the last column. Table II provides details on the computational mesh and the corresponding resolutions in terms of conventional wall scaling (Δx^+, Δy_w^+, Δz^+) and semi-local scaling at the channel center (Δx_c^*, Δy_c^*, Δz_c^*). It can be seen that an adequate mesh resolution is achieved for all cases.

Next, the abbreviations and the choice of ρ and μ variations for the simulated cases are motivated. The constant properties with $Re_\tau(h^+) = 395$ are abbreviated as CP395. CRe_τ^* refers to a case where $Re_\tau^* = Re_\tau$ across the whole channel height. This is achieved with ρ and μ being proportional to $1/T$ and $\sqrt{1/T}$, respectively. Such a behaviour can qualitatively occur in fluids at supercritical pressures close to the pseudo-critical point; both ρ and μ decrease with increase of temperature.[23] GL corresponds to a gas-like property variation, whereby ρ decreases and μ increases with increase of T. LL corresponds to a liquid-like behaviour as μ deceases with increase of T. Cν refers to a constant kinematic viscosity ν case with $\rho(T) = \mu(T)$. Finally, $SRe_{\tau C\nu}^*$ and $SRe_{\tau GL}^*$ are hypothetical cases that resemble similar Re_τ^* profiles as cases Cν and GL, respectively, but with different functional relations for ρ and μ. Both cases are studied to show that flows with similar Re_τ^* profiles, irrespective of density and viscosity variations, show similar turbulent characteristics.

Figure 1 shows the variation of properties and Re_τ^* for all cases. Considerable variations in both ρ and μ are obtained. Also, it can be seen that Re_τ^* changes by almost a factor of 2 across the channel for case GL, $SRe_{\tau GL}^*$ (395 at wall to $\approx$ 150 at center), and LL (395 at wall to $\approx$ 700 at center). Re_τ^* for case CRe_τ^* is by definition constant across the complete channel height. The quasi-similar Re_τ^*

TABLE I. Flow parameters for all cases. CP395—Constant Property case with $Re_\tau(h^+) = 395$; CRe_τ^*—variable property case with Constant Re_τ^* ($= Re_\tau$) across the channel; GL—case with Gas-Like property variations; LL—case with Liquid-Like property variations; Cν—variable property case with Constant kinematic viscosity ν; $SRe_{\tau C\nu}^*$—variable property case with Re_τ^* Similar to case Cν; $SRe_{\tau GL}^*$— variable property case with Re_τ^* Similar to case GL.

Case	ρ	μ	h^*
CP395	1	1	395
CRe_τ^*	$1/T$	$1/\sqrt{T}$	395
GL	$1/T$	$T^{0.7}$	142
LL	1	$1/T$	703
Cν	$1/T$	$1/T$	538
$SRe_{\tau C\nu}^*$	1	$1/\sqrt{T}$	532
$SRe_{\tau GL}^*$	1	$T^{1.2}$	152

TABLE II. Mesh resolution for all cases.

Case	N_x	N_y	N_z	Δx^+	Δy_w^+	Δz^+	Δx_c^*	Δy_c^*	Δz_c^*
CP395	240	264	240	10.34	1.03	5.17	10.34	4.01	5.17
CRe_τ^*	240	264	240	10.34	1.03	5.17	10.34	4.01	5.17
GL	360	264	360	17.23	1.03	6.89	6.20	1.44	2.48
LL	360	360	360	6.89	0.69	3.45	12.27	5.28	6.13
$\mathrm{C}\nu$	240	312	240	10.34	0.80	5.17	14.08	4.66	7.04
$\mathrm{SRe}_{\tau C\nu}^*$	240	312	240	10.34	0.80	5.17	13.92	4.61	6.96
$\mathrm{SRe}_{\tau GL}^*$	360	264	360	17.23	1.03	6.89	6.63	1.54	2.65

profiles for cases—GL, $\mathrm{SRe}_{\tau GL}^*$ and $\mathrm{C}\nu$, $\mathrm{SRe}_{\tau C\nu}^*$ can also be seen in Figure 1(c). The quasi-similar Re_τ^* profiles are obtained for both pairs using different combinations of ρ and μ (also shown in Figures 1(a) and 1(b)).

For all simulations λ and c_p are considered to be constant, the reference Reynolds number $Re_\tau(h^+)$ and Prandtl number Pr_w in Equations (2) and (3) are set to 395 and unity, respectively, and the flow is driven by a constant stream-wise pressure gradient. The volumetric heat flux ϕ in Equation (3) is 18.55 for case $\mathrm{SRe}_{\tau GL}^*$, 16 for case $\mathrm{C}\nu$, and 17.55 for the other cases. The value of ϕ is chosen such that strong variations in properties occur, but without considerably invalidating Morkovin's hypothesis—both $\sqrt{\overline{\rho'^2}}/\overline{\rho}$ and $\sqrt{\overline{\mu'^2}}/\overline{\mu}$ are less than 0.15 for all cases, as can be seen from Figure 2. The reason for different ϕ values for cases $\mathrm{SRe}_{\tau GL}^*$ and $\mathrm{C}\nu$ is to obtain quasi-similar
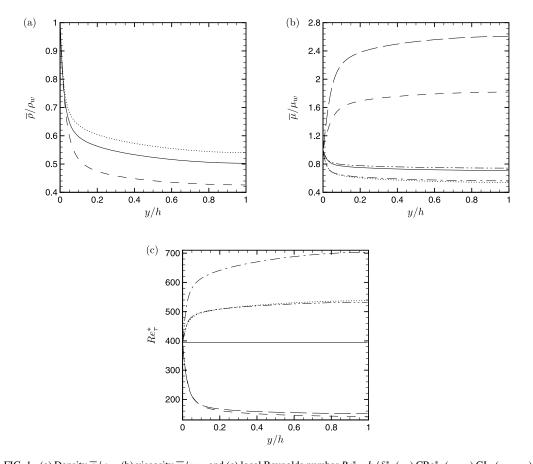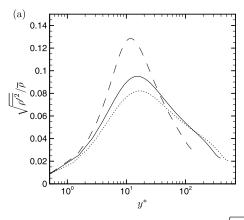

FIG. 1. (a) Density $\overline{\rho}/\rho_w$, (b) viscosity $\overline{\mu}/\mu_w$, and (c) local Reynolds number $Re_\tau^* = h/\delta_v^*$. (—) CRe_τ^*, (- - - -) GL, (— · —) LL, (······) $\mathrm{C}\nu$, (— · · —) $\mathrm{SRe}_{\tau C\nu}^*$, (— —) $\mathrm{SRe}_{\tau GL}^*$.

FIG. 2. Root mean square of (a) density fluctuations $\sqrt{\overline{\rho'^2}}/\overline{\rho}$, (b) viscosity fluctuations $\sqrt{\overline{\mu'^2}}/\overline{\mu}$. Lines are the same as in Figure 1.

Re_τ^* profiles with respect to cases GL and $SRe_{\tau C\nu}^*$, respectively. The domain size $L_x \times L_y \times L_z$ of the channel for cases GL and $SRe_{\tau GL}^*$ is $5\pi h \times 2h \times 2\pi h$, while for the other cases the domain size is $2\pi h \times 2h \times \pi h$. It should be noted that $Pr_w = 1$ was chosen to isolate the effects of density and viscosity only. Moreover, $Pr_w = 1$ ensures sufficiently large temperature gradients, but small enough to not invalidate Morkovin's hypothesis.

IV. RESULTS

In Section IV A, the semi-local scaling of turbulent statistics in wall bounded flows with variable properties is investigated. Three simulation pairs are compared to assess this scaling: case CRe_τ^* with case CP395, case $SRe_{\tau GL}^*$ with case GL, and case $SRe_{\tau C\nu}^*$ with case $C\nu$. The reasons for using the above three pairs are motivated and implications of using the semi-local scaling are discussed. In Section IV B, the results of cases GL and LL are compared with the constant property cases at different Reynolds number to highlight variable property effects.

A. Semi-local scaling of turbulent statistics under variable property conditions

In this section we assess the arguments made in Sections II B and II C using the DNS results for three pairs of simulations. The validity of Morkovin's hypothesis which was used in Section II C to develop the theoretical framework is also assessed. The first pair is CRe_τ^* and CP395. Because of the functional relation of ρ and μ for case CRe_τ^*, Re_τ^* is a constant and equal to 395 across the whole channel height. Consequently, the semi-local inner co-ordinate y^* equals the classical inner co-ordinate y^+ and Equation (7) is equivalent to Equation (5), with Re_τ^* approaching Re_τ. The other two pairs involve comparison among variable property cases with similar Re_τ^*, but different density and viscosity profiles. The case $SRe_{\tau GL}^*$ represents a case wherein density is constant, and the viscosity varies such that the Re_τ^* remains approximately similar to that of case GL (see Figure 1). A similar comparison for case $SRe_{\tau C\nu}^*$ and $C\nu$, with approximately similar Re_τ^* profiles obtained using different combinations of ρ and μ is performed.

Based on Equation (20), three quasi-similar Re_τ^* pairs are assessed for quasi-similarity of van Driest transformed stream-wise velocity profile $\overline{u}^{vd}$ and the Reynolds shear stress $\overline{\rho u''v''}/\tau_w$. The comparison of $\overline{u}^{vd}$ is shown in Figure 3. The solid line indicates the stream-wise velocity profile for variable density cases (CRe_τ^*, GL, and $C\nu$), while the dashed line represents their corresponding van Driest transformed stream-wise velocity profile. $\overline{u}^{vd}$ overlaps with the velocity from the corresponding quasi-similar Re_τ^* cases (symbols) with constant density (CP395, $SRe_{\tau GL}^*$, and $SRe_{\tau C\nu}^*$). The comparison of the Reynolds shear stress is shown in Figures 4(a)-4(c) also showing a good collapse. Comparison of other second order statistics, namely, normal Reynolds stress components $\overline{\rho u_i''u_i''}/\tau_w$, their corresponding anisotropies b_{ii}, and the root mean square of pressure fluctuations p_{rms}'/τ_w is shown in Figures 4(d)-4(l). The normalised anisotropy tensor is defined
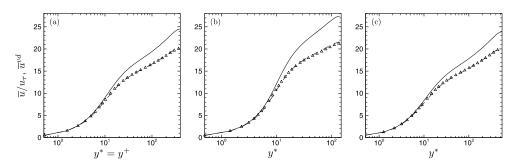
FIG. 3. Averaged velocity profiles for cases (a) CP395 and CRe^*_τ, (b) $SRe^*_{\tau GL}$ and GL, (c) $SRe^*_{\tau C\nu}$ and $C\nu$. Symbols are constant density cases: CP395, $SRe^*_{\tau GL}$, and $SRe^*_{\tau C\nu}$, lines are variable density cases: CRe^*_τ, GL, and $C\nu$. (—) mean stream-wise velocity $\overline{u}/u_\tau$ and (- - - -) van Driest transformed stream-wise velocity profile $\overline{u}^{vd}$.
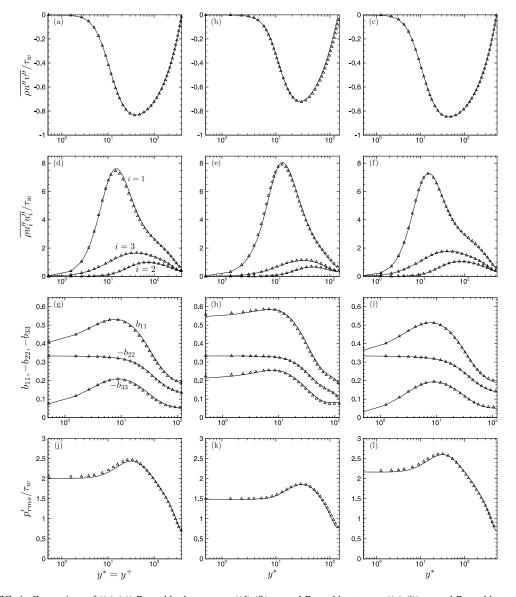

FIG. 4. Comparison of ((a)-(c)) Reynolds shear stress, ((d)-(f)) normal Reynolds stresses, ((g)-(i)) normal Reynolds stress anisotropies, and ((j)-(l)) root mean square of pressure fluctuations for cases (left column) CP395 and CRe^*_τ, (middle column) $SRe^*_{\tau GL}$ and GL, (right column) $SRe^*_{\tau C\nu}$ and $C\nu$. Symbols are constant density cases: CP395, $SRe^*_{\tau GL}$, and $SRe^*_{\tau C\nu}$, lines are variable density cases: CRe^*_τ, GL, and $C\nu$.

FIG. 5. Comparison of pre-multiplied 1D ((a)-(c)) stream-wise spectra and ((d)-(f)) span-wise spectra of $\overline{\rho u''u''}/\tau_w$ at $y^* \approx 15$ for cases (left column) CP395 and CRe_τ^*, (middle column) $SRe_{\tau GL}^*$ and GL, (right column) $SRe_{\tau C\nu}^*$ and $C\nu$. Symbols are constant density cases: CP395, $SRe_{\tau GL}^*$, and $SRe_{\tau C\nu}^*$, lines are variable density cases: CRe_τ^*, GL, and $C\nu$. In ((a)-(c)), the inset shows the 1D stream-wise energy spectra in log-log plot.

as $b_{ij} = \overline{\rho u_i''u_j''}/\overline{\rho u_k''u_k''} - 1/3\delta_{ij}$. All comparisons support the universality of the second order turbulent statistics for quasi-similar Re_τ^* cases. We further investigate the quasi-similarity of the 1D energy spectra in Figures 5(a)-5(f). Figures 5(a)-5(c) show the pre-multiplied stream-wise 1D spectra of $\overline{\rho u''u''}/\tau_w$ at $y^* \approx 15$ as a function of semi-locally scaled ($k_x^* = k_x/Re_\tau^*$) wave-number for quasi-similar Re_τ^* cases. The inset shows the energy spectra in log-log plot, showing adequacy of grid-resolution as energy falls off over several decades. Because of moderate Reynolds number, the inertial range is not very prominent (shown by $k_x^{-5/3}slope$). Span-wise 1D spectra are compared in Figures 5(d)-5(f). Both stream-wise and span-wise spectra show good collapse for quasi-similar Re_τ^* cases. Figures 3–5 provide evidence that the semi-local scaling is an effective tool to categorize variable property turbulence.

We now proceed to assess the influence of density fluctuations on turbulent statistics (Morkovin's hypothesis) by investigating second, third, and fourth order moments of velocity fluctuation. Using Equation (14), an exact definition for re-scaled second order turbulent statistics is $\overline{\hat{u}_i'\hat{u}_j'} = \overline{\rho u_i'u_j'}/\tau_w$. However, in Figures 4(a)-4(i) we use $\overline{\rho u_i''u_j''}/\tau_w$ to test the quasi-similarity of second-order statistics assuming that under the limit of small density fluctuations $\overline{\hat{u}_i'\hat{u}_j'} = \overline{\rho u_i'u_j'}/\tau_w \approx \overline{\rho u_i''u_j''}/\tau_w \approx \overline{\rho u_i''u_j''}/\tau_w$ should hold. The different statistics are related as

$$\overline{\rho u_i''u_i''} = \overline{\rho}\,\overline{u_i''u_i''} + \overline{\rho'u_i''u_i''}, \tag{23}$$

and using Equation (13) the relation between Reynolds and Favre averaged second order statistics is given as

$$\overline{\rho}\,\overline{u_i'u_i'} = \overline{\rho u_i''u_i''} - \overline{\rho}\left(\frac{\overline{\rho'u_i'}}{\overline{\rho}}\right)^2. \tag{24}$$

These different relations are plotted in Figures 6(a)-6(c), where it can be seen that the differences are negligible. The maximum error of $\approx 3.5\%$ occurs in case GL for which the density fluctuations are the highest (see Figure 2(a)). The second terms on the right hand side of Equation (23) and (24) are negligible compared with the first terms and therefore the difference between the profiles is insignificant. The above result reinforces the use of Morkovin's hypothesis in Section II C.
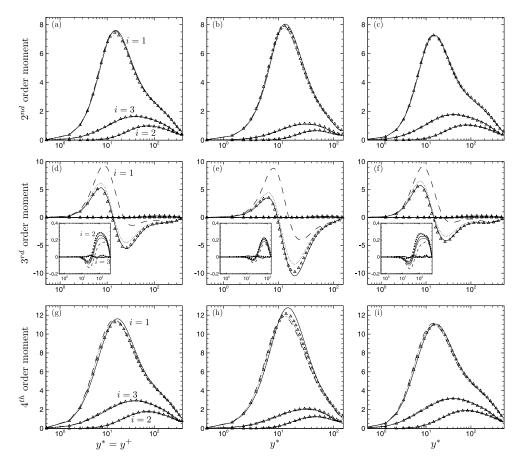
FIG. 6. Influence of density fluctuation on ((a)-(c)) second, ((d)-(f)) third, and ((g)-(i)) fourth order moments of velocity fluctuations for cases (left column) CP395 and CRe_τ^*, (middle column) $\text{SRe}_{\tau GL}^*$ and GL, (right column) $\text{SRe}_{\tau C\nu}^*$ and Cν. Symbols are constant density cases: CP395, $\text{SRe}_{\tau GL}^*$, and $\text{SRe}_{\tau C\nu}^*$, lines are variable density cases: CRe_τ^*, GL, and Cν. In ((a)-(c)) (—) $\overline{\rho u_i'' u_i''}/\tau_w$, (- - - -) $\overline{\rho} \overline{u_i'' u_i''}/\tau_w$, (······) $\overline{\rho} \overline{u_i' u_i'}/\tau_w$. In ((d)-(f)) (—) $\overline{\rho^{3/2} u_i'' u_i'' u_i''}/\tau_w^{3/2}$, (- - - -) $\overline{\rho}^{3/2} \overline{u_i'' u_i'' u_i''}/\tau_w^{3/2}$, (······) $\overline{\rho}^{3/2} \overline{u_i' u_i' u_i'}/\tau_w^{3/2}$. In ((g)-(i)) (—) $\sqrt{\overline{\rho^2 u_i'' u_i'' u_i'' u_i''}}/\tau_w$, (- - - -) $\overline{\rho}\sqrt{\overline{u_i'' u_i'' u_i'' u_i''}}/\tau_w$, (······) $\overline{\rho}\sqrt{\overline{u_i' u_i' u_i' u_i'}}/\tau_w$.

We further assess the quasi-similarity and applicability of Morkovin's hypothesis on third and fourth order moments of velocity fluctuations. Using Equation (14), the third and fourth order moments can be expressed as $\overline{\hat{u}_i' \hat{u}_i' \hat{u}_i'} = \overline{\rho}^{3/2} \overline{u_i' u_i' u_i'}/\tau_w^{3/2}$ and $\overline{\hat{u}_i' \hat{u}_i' \hat{u}_i' \hat{u}_i'} = \overline{\rho}^2 \overline{u_i' u_i' u_i' u_i'}/\tau_w^2$, respectively. Under the validity of Morkovin's hypothesis, these statistics should satisfy the following relation for the third order $\overline{\hat{u}_i' \hat{u}_i' \hat{u}_i'} = \overline{\rho}^{3/2} \overline{u_i' u_i' u_i'}/\tau_w^{3/2} \approx \overline{\rho}^{3/2} \overline{u_i'' u_i'' u_i''}/\tau_w^{3/2} \approx \overline{\rho^{3/2} u_i'' u_i'' u_i''}/\tau_w^{3/2}$ and $\overline{\hat{u}_i' \hat{u}_i' \hat{u}_i' \hat{u}_i'} = \overline{\rho}^2 \overline{u_i' u_i' u_i' u_i'}/\tau_w^2 \approx \overline{\rho}^2 \overline{u_i'' u_i'' u_i'' u_i''}/\tau_w^2 \approx \overline{\rho^2 u_i'' u_i'' u_i'' u_i''}/\tau_w^2$ for the fourth order moments. For third order moments, the relation between $\overline{\rho^{\frac{3}{2}} u_i'' u_i'' u_i''}$ and $\overline{\rho}^{\frac{3}{2}} \overline{u_i'' u_i'' u_i''}$ can be expressed by using a binomial series for $\rho^{3/2} = \overline{\rho}^{3/2}(1 + \rho'/\overline{\rho})^{3/2}$, leading to

$$\overline{\rho^{\frac{3}{2}} u_i'' u_i'' u_i''} \approx \overline{\rho}^{\frac{3}{2}} \overline{u_i'' u_i'' u_i''} + \frac{3}{2} \overline{\rho' u_i'' u_i'' u_i''}. \tag{25}$$

Using Equation (13), the relation between Reynolds and Favre averaged third order statistics is then

$$\overline{\rho}^{\frac{3}{2}} \overline{u_i' u_i' u_i'} = \overline{\rho}^{\frac{3}{2}} \overline{u_i'' u_i'' u_i''} + 3\overline{\rho}^{\frac{3}{2}} \left(\frac{\overline{\rho' u_i'}}{\overline{\rho}}\right) \overline{u_i'' u_i''} - 2\overline{\rho}^{\frac{3}{2}} \left(\frac{\overline{\rho' u_i'}}{\overline{\rho}}\right)^3. \tag{26}$$

Similarly, for fourth order moments, the relation between $\overline{\rho^2 u_i'' u_i'' u_i'' u_i''}$ and $\overline{\rho}^2 \overline{u_i'' u_i'' u_i'' u_i''}$ is

$$\overline{\rho^2 u_i'' u_i'' u_i'' u_i''} = \overline{\rho}^2 \overline{u_i'' u_i'' u_i'' u_i''} + 2\overline{\rho}\overline{\rho' u_i'' u_i'' u_i'' u_i''} + \overline{\rho' \rho' u_i'' u_i'' u_i'' u_i''}, \tag{27}$$

and using Equation (13) the relation between Reynolds and Favre averaged fourth order statistics is given as

$$\overline{\rho}^2\overline{u_i'u_i'u_i'u_i'} = \overline{\rho}^2\overline{u_i''u_i''u_i''u_i''} + 4\overline{\rho}^2\left(\frac{\overline{\rho'u_i'}}{\overline{\rho}}\right)\overline{u_i''u_i''u_i''} + 6\overline{\rho}^2\left(\frac{\overline{\rho'u_i'}}{\overline{\rho}}\right)^2\overline{u_i''u_i''} - 3\overline{\rho}^2\left(\frac{\overline{\rho'u_i'}}{\overline{\rho}}\right)^4. \tag{28}$$

Figures 6(d)-6(f) show the comparison for the third order moments of velocity fluctuations between quasi-similar Re_τ^* cases. The inset shows an enlarged view for wall-normal (i = 2) and span-wise direction (i = 3). Unlike the lower-order statistics, the adequacy of the sample size used to compute the higher-order statistics is marginal as can be seen by small oscillations in the profiles of span-wise third order moments, which should be zero. For the variable density cases (CRe$_\tau^*$, GL and Cν), the third order statistics using different forms of averaging do not collapse, which indeed is a breakdown of Morkovin's hypothesis. This breakdown will most likely also be present in fully compressible simulations, but to the best of the authors knowledge, there is no literature that studies the Morkovin's hypothesis for third order statistics in compressible flows. Interestingly, a good agreement between quasi-similar Re_τ^* cases is obtained using $\overline{\rho^{3/2}u_i''u_i''u_i''}/\tau_w^{3/2}$. The comparison is only qualitatively similar when $\overline{\rho}^{3/2}\overline{u_i'u_i'u_i'}/\tau_w^{3/2}$ is used but different when $\overline{\rho}^{3/2}\overline{u_i''u_i''u_i''}/\tau_w^{3/2}$ is used. These results indicate that $\sqrt{\rho}u_i''/\sqrt{\tau_w}$ is the appropriate scale for comparing quasi-similarity of third moments. The reason for the breakdown of Morkovin's hypothesis is discussed next. For the stream-wise component (i = 1), the third order moments are a measure of low and high speed streaks. In our present simulations with a cooled wall, the turbulent heat transfer at the lower wall requires $T'v' < 0$. Based on quadrant analysis, it is known that the high speed streaks have a tendency to move towards the wall (sweep) while low speed streaks tend to lift away from the wall (ejection), which for the lower wall corresponds to $u'v' < 0$. This implies that $T'u' > 0$, and since the density is inversely proportional to temperature $\rho'u' < 0$. The terms $\overline{\rho'u''u''u''}$ and $\overline{\rho'u'}$ are a measure of preferential concentration of high density fluid in low speed streaks and low density fluid in high speed streaks. In Equation (25), this measure of preferential concentration is dominant as both the first and second terms on the right hand side are of comparable magnitudes, thereby causing a significant difference between $\overline{\rho^{\frac{3}{2}}u''u''u''}$ and $\overline{\rho}^{\frac{3}{2}}\overline{u''u''u''}$. Similarly, the second term on the right hand side of Equation (26) is of the same order as the first one, therefore, resulting in the difference between $\overline{\rho}^{3/2}\overline{u'u'u'}$ and $\overline{\rho}^{3/2}\overline{u''u''u''}$.

Figures 6(g)-6(i) show the comparison for the square root of the fourth order moment of velocity fluctuations. A good collapse is obtained for all cases except case GL for which a maximum difference of ≈9% occurs due to the high magnitudes of density fluctuations (see Figure 2(a)). In both Equations (27) and (28), the first term on the right side is dominant, therefore making the statistic weakly dependent on density fluctuations.

B. Turbulence modulation with respect to constant property flows

1. Turbulent statistics

Cases GL and LL are compared to data from constant property turbulent flows to investigate the effect of variable properties on turbulent statistics. In order to distinguish Reynolds number effects, the constant property cases are chosen such that the Re_τ^* distribution of cases GL and LL is approximately bounded between two corresponding constant property cases. Figure 7(a) shows the comparison of normal Reynolds stresses as a function of y^+ for case GL with constant property cases CP395 ($Re_\tau = 395$) and a case of Iwamoto, Suzuki, and Kasagi[32] with $Re_\tau = 150$. A similar comparison is shown for case LL in Figure 7(b), whereby the reference data are taken from CP395 and from Iwamoto, Suzuki, and Kasagi[32] with $Re_\tau = 650$. As observed in previous studies,[10,14,15] the use of the traditional y^+ wall scaling fails to provide a collapse of the data. Figure 8 shows the same plot using the semi-local scaling y^*, which gives a better collapse of the data as the peak locations occur at similar y^* values for all cases. Interestingly, the stream-wise component increases for case GL in comparison to both CP395 and $Re_\tau = 150$. Similarly for case LL, the stream-wise component decreases with respect to CP395 and $Re_\tau = 650$. It can also be seen that
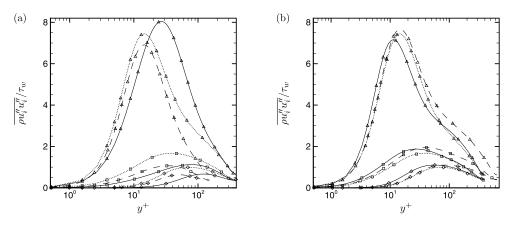
FIG. 7. Profiles of normal Reynolds stresses as a function of y^+ for (a) case GL and (b) case LL, compared to CP395 and Iwamoto, Suzuki, and Kasagi.[32] In (a) and (b): ($\triangle$) $\overline{\rho u''u''}/\tau_w$, ($\diamond$) $\overline{\rho v''v''}/\tau_w$, ($\square$) $\overline{\rho w''w''}/\tau_w$. In (a), (—) case GL and (- - - -) $h^+ = 150$ from Iwamoto, Suzuki, and Kasagi.[32] In (b), (—) case LL and (- - - -) $h^+ = 650$ from Iwamoto, Suzuki, and Kasagi.[32] (······) case CP395.

for case GL the span-wise and wall-normal Reynolds stresses decrease with respect to CP395. The opposite is true for case LL. This increase (decrease) in the stream-wise anisotropy for case GL (LL) is shown in Figure 9 as a function of y^*. It shows that the increase (decrease) of stream-wise anisotropy for case GL (LL) is accompanied with the increase (decrease) of span-wise anisotropy. The wall-normal anisotropy seems to be unaffected for all cases, irrespective of Reynolds number or property variations. Thus, the principal axes for the Reynolds stress tensor become more aligned with the mean flow direction for case GL, while the opposite occurs for case LL. Foysi, Sarkar, and Friedrich[15] attributed the increase of anisotropy in their compressible air flow simulations to the fact that density has a non-local effect on the pressure-strain correlation. However, as can be seen from Figure 4(h), a similar increase in anisotropy also occurs for a turbulent flow with constant density, but increasing viscosity towards the channel center. Figures 10 and 11 show the Reynolds shear stress in outer and inner scales, respectively. To highlight the differences in terms of Reynolds shear stress $\overline{\rho u''v''}/\tau_w$, their profiles are plotted as a function of y/h in Figure 10. It can be seen that $\overline{\rho u''v''}/\tau_w$ remains bounded between the two constant property cases near the wall, while towards the channel core the expected linear profile is obtained. Taking into account the low-Reynolds number effect for case GL, a good approximate collapse is obtained for the inner scaled Reynolds stress in Figure 11. Another point worth noting is the cross-over of the Reynolds shear stress from the variable property with the constant property turbulent flows with $Re_\tau^* = 150$ and 650, respectively, because of changes in anisotropy for cases GL and LL.
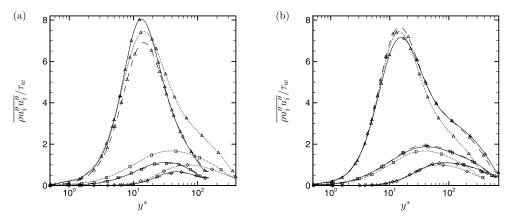

FIG. 8. Profiles of normal Reynolds stresses as a function of y^* for (a) case GL and (b) case LL, compared to CP395 and Iwamoto, Suzuki, and Kasagi.[32] Lines and symbols are the same as in Figure 7.
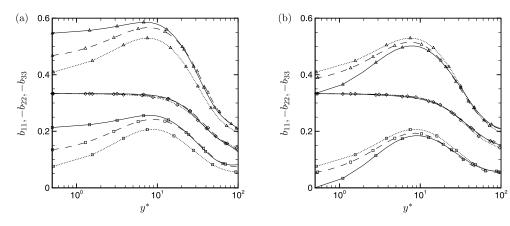
FIG. 9. Profiles of normal Reynolds stress anisotropies as a function of y^* for (a) case GL and (b) case LL, compared to CP395 and Iwamoto, Suzuki, and Kasagi.[32] In (a) and (b): ($\triangle$) b_{11}, ($\diamond$) b_{22}, ($\square$) b_{33}. Lines are the same as in Figure 7.

2. Near-wall turbulent structures

The modulation of variable property turbulent statistics is further substantiated by means of near-wall turbulent structures. Coleman, Kim, and Moser,[10] Duan, Beekman, and Martin,[11] Lagha *et al.*,[12] observed increased stream-wise coherence (longer streaks) for supersonic turbulent boundary layers with cooled walls, while shorter streaks were observed for heated walls by Duan, Beekman, and Martin.[11] These streak modifications were quantified in terms of wall based viscous units. Morinishi, Tamano, and Nakabayashi[13] used two-point correlations to conclude that near-wall streaks do not become more coherent and are independent of heated or cooled walls, when semi-local scaling is taken into account. Coleman, Kim, and Moser[10] explained the occurrence of elongated streaks by the change of turbulence-to-mean time scale ratio. However, Morinishi, Tamano, and Nakabayashi[13] and Duan, Beekman, and Martin[11] found that there was no connection between near-wall streak structures and time scale ratio, as no significant changes in the time scale ratio occurred.

In order to clarify these inconsistent observations, we revisit some of these conclusions and in addition provide further insights into turbulence modulation, by examining 1D stream-wise and span-wise energy spectra, turbulence-to-mean time scale ratio, pressure-strain to production ratio, contour plots of $\sqrt{\rho}u''/\sqrt{\tau_w}$ and joint-probability density functions (pdfs) for $\sqrt{\rho}u''/\sqrt{\tau_w}$ and $\sqrt{\rho}v''/\sqrt{\tau_w}$. Figure 12 shows the pre-multiplied stream-wise 1D spectra of $\overline{\rho u''u''}/\tau_w$ at the location of their peak at $y^* \approx 15$ as a function of both semi-locally ($k_x^* = k_x/Re_\tau^*$) and classically scaled ($k_x^+ = k_x/Re_\tau$) wave-numbers. Using the classically scaled co-ordinates, it can be seen that the spectra for case GL are shifted to lower wave-numbers, while they are shifted to higher wave-numbers for case LL (see solid lines with and without symbols). Thus, the structures appear
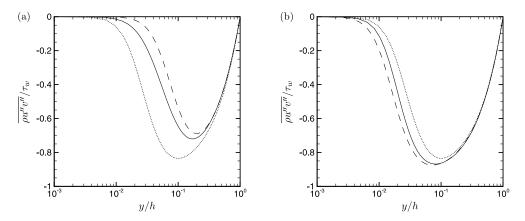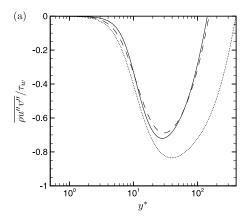

FIG. 10. Reynolds shear stress $\overline{\rho u''v''}/\tau_w$ for (a) case GL and (b) case LL, against y/h. Lines are the same as in Figure 7.
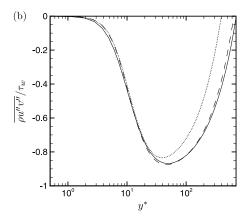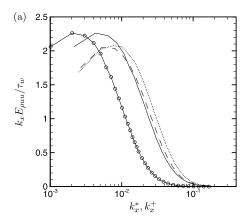
FIG. 11. Reynolds shear stress $\overline{\rho u'' v''}/\tau_w$ for (a) case GL and (b) case LL, against y^*. Lines are the same as in Figure 7.

elongated for case GL and shortened for case LL, as also concluded by Coleman, Kim, and Moser,[10] Duan, Beekman, and Martin,[11] Lagha *et al.*[12] However, using semi-local co-ordinates, an approximate collapse over a wide wave-number range can be obtained, and the peaks of $E_{\overline{\rho u'' u''}}/\tau_w$ occur at approximately the same k_x^* location for both cases (note, the peak of $E_{\overline{\rho u'' u''}}/\tau_w$ for CP395 (dotted line) in Figure 12(a) is at a slightly higher wave-number due to low-Reynolds number effects for cases GL and Iwamoto, Suzuki, and Kasagi[32] with $Re_\tau = 150$). Additionally, Figure 13 shows the pre-multiplied span-wise 1D spectra for $\overline{\rho u'' u''}/\tau_w$ at the same y^* location as a function of k_z^* and k_z^+, to emphasize that also the mean spacing of stream-wise streaks remains unaltered as a function of k_z^*. In other words, the modulation of turbulence (longer or shorter streaks) observed at $y^* \approx 15$ using classical wall scaling is misleading and exclusively quantified by semi-local scales only.

The pre-multiplied spectra provide additional insights with respect to previous findings. It can be seen that for case GL the energy containing low wave-number scales strengthen (see peak magnitude of $E_{\overline{\rho u'' u''}}/\tau_w$), while they weaken for case LL. The pre-multiplied stream-wise 1D spectra of $\overline{\rho u'' u''}/\tau_w$ at $y^* \approx 15$ for case $SRe_{\tau GL}^*$ (see Figure 5(b)) exhibited similar strengthening at large wavelengths as case GL. The strengthening and weakening of these large scale anisotropic structures seems to be independent of individual density or viscosity profiles, and thus depend on the Re_τ^* profile only. The previously mentioned increased (decreased) stream-wise Reynolds stress for case GL (LL) is associated with strengthening (weakening) of these large-scale stream-wise structures.

The turbulence-to-mean time scale ratio $S^* = \overline{\rho u_k'' u_k''} S/(2\epsilon)$, with $S = \partial_y \bar{u}$ the mean strain rate, $\epsilon = -\overline{\tau_{ij}' \partial_{x_j} u_i''}$ the turbulent kinetic energy dissipation, and $\tau_{ij}' = \tau_{ij} - \overline{\tau}_{ij}$ the fluctuating viscous stress tensor, is plotted as a function of y^* in Figure 14(a) for cases GL and LL, and compared with
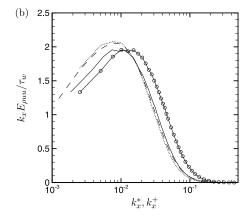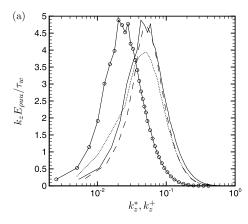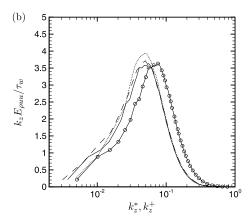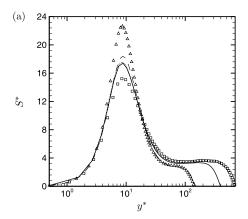

FIG. 12. Comparison of pre-multiplied 1D stream-wise spectra of $\overline{\rho u'' u''}/\tau_w$ at $y^* \approx 15$ for (a) case GL and (b) case LL. Lines with symbols are plotted as function of k_x^+, while lines without symbols are plotted as function of k_x^*. Lines are the same as in Figure 7.

FIG. 13.   Comparison of pre-multiplied 1D span-wise spectra of $\overline{\rho u'' u''}/\tau_w$ at $y^* \approx 15$ for (a) case GL and (b) case LL. Lines with symbols are plotted as function of k_z^+, while lines without symbols are plotted as function of k_z^*. Lines are the same as in Figure 7.

constant property cases CP395 and data from Iwamoto, Suzuki, and Kasagi[32] with $Re_\tau = 150$ and $Re_\tau = 650$. It can be seen that at $y^* \approx 8$ the turbulence-to-mean time scale ratio S^* has increased for case GL, while it has decreased for case LL when compared to the constant property cases that have similar peak values. Thus, the changes of S^* are an indication for the modification of near-wall structure. This modified time scale results in a more anisotropic turbulence for case GL with higher S^*, and less anisotropic turbulence for case LL with smaller S^*.

The increased (decreased) anisotropy for case GL (LL) is related to strengthening (weakening) of large-scale streaks and can be associated with changes in energy transfer from stream-wise to other directions. The pressure-strain term $\overline{2p' d_x u''}$, which is responsible for this exchange is modified. The negative ratio of pressure-strain to stream-wise production rate $\pi^* = \overline{2p' d_x u''} / -2\overline{\rho u'' v''} d_y \tilde{u}$ is shown in Figure 14(b) and compared with constant property cases. A clear decrease (increase) in pressure-strain for case GL (LL) can be observed in the near-wall region. In fact, this modulation in time scale and energy transfer ratios have their origin in the viscous term of Equation (22) as Re_τ^* varies across the wall normal direction.

A visual impression of these large scale structures can be obtained by means of contour plots of instantaneous flow fields as given in Figures 15 and 16. Figure 15 shows stream-wise velocity fluctuations $\sqrt{\rho} u''/\sqrt{\tau_w}$ in a plane parallel to the wall at $y^* \approx 15$ for case CP395, LL, and $SRe_{\tau GL}^*$. Even though all three cases are constant density flows (see Table I), we suggest to use ρ, instead of $\overline{\rho}$, for the normalization ($\sqrt{\rho} u''/\sqrt{\tau_w}$) in these plots. The reason for this is that the magnitude of the streaks is modulated by the preferential concentration of high density fluid in a
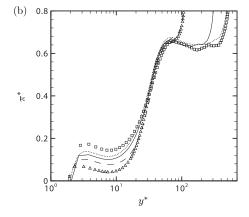

FIG. 14.   (a) The turbulence-to-mean time scale ratio S^* and (b) pressure strain to production ratio π^* of $\overline{\rho u'' u''}/\tau_w$ for case GL and case LL, compared with CP395 and Iwamoto, Suzuki, and Kasagi.[32] ($\triangle$) case GL, ($\square$) case LL, (—) case CP395, (- - - -) $h^+ = 150$ from Iwamoto, Suzuki, and Kasagi[32] and (······) $h^+ = 650$ from Iwamoto, Suzuki, and Kasagi.[32]
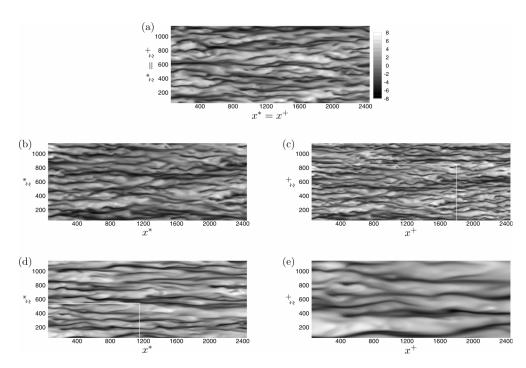
FIG. 15. Instantaneous stream-wise velocity fluctuations $\sqrt{\rho}u''/\sqrt{\tau_w}$ in an $x - z$ plane at $y^* \approx 15$. (a) Case CP395, (b) case LL using $x^* - z^*$ co-ordinates, (c) case LL using $x^+ - z^+$ co-ordinates, (d) case $\mathrm{SRe}^*_{\tau GL}$ using $x^* - z^*$ co-ordinates, and (e) case $\mathrm{SRe}^*_{\tau GL}$ using $x^+ - z^+$ co-ordinates. The white box in (c) corresponds to (b) and box in (d) corresponds to (e).

low-speed streak, and vice versa (see discussion for Figures 6(d)-6(f)). For cases LL and $\mathrm{SRe}^*_{\tau GL}$, both semi-local ($x^* = xRe^*_\tau$ and $z^* = zRe^*_\tau$) and classical ($x^+ = xRe_\tau$ and $z^+ = zRe_\tau$) wall units are shown. The box size in all visualisations is 2400×1100, based on corresponding non-dimensional co-ordinates $x^* \times z^*/x^+ \times z^+$. Scale separation becomes more prominent for case LL (Figures 15(b) and 15(c)) and less prominent for case $\mathrm{SRe}^*_{\tau GL}$ (Figures 15(d) and 15(e)) when compared with the constant property case (Figure 15(a)). The comparison of semi-locally scaled variable property contours (Figures 15(b) and 15(d)) with constant property contours (Figure 15(a)) shows a similar mean span-wise spacing between the streaks for all cases. A similar comparison using classical wall co-ordinates (Figures 15(c) and 15(e)) shows decreased spacing for case LL, and an increased spacing for case $\mathrm{SRe}^*_{\tau GL}$. The white box in Figures 15(c) and 15(d) indicates the domain size of
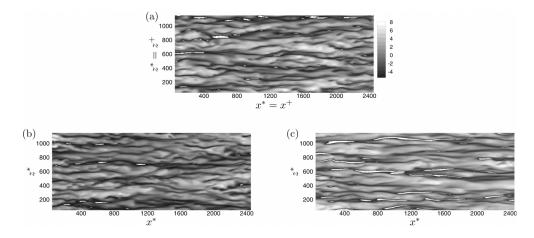

FIG. 16. Instantaneous stream-wise velocity fluctuations $\sqrt{\rho}u''/\sqrt{\tau_w}$ in $x^* - z^*$ plane at $y^* \approx 15$. Contour for $\sqrt{\rho}u''/\sqrt{\tau_w} < -5.5$ are cut-off (seen as white). (a) Case CP395, (b) case LL, (c) case $\mathrm{SRe}^*_{\tau GL}$.

Figures 15(b) and 15(e), respectively, in order to outline the scaling of the structures. The strengthening ($Re_\tau^* < Re_\tau$ in channel core) and weakening ($Re_\tau^* > Re_\tau$ in channel core) of near-wall structures with respect to the constant property case can be visualised in Figure 16. The $\sqrt{\rho}u''/\sqrt{\tau_w}$ contours are taken at the same plane and time as Figure 15. The low-speed streaks are cut-off below a threshold value of $\sqrt{\rho}u''/\sqrt{\tau_w} = -5.5$, thus highlighting the more energetic structures. It can be seen that for case LL (Figure 16(b)) the energetic spots reduce in comparison to case CP395 (Figure 16(a)). On the other hand, the energetic spots in case of $SRe_{\tau GL}^*$ (Figure 16(c)) become more prominent. The large-scale stream-wise structures are low-speed streaks which become strengthened (weakened) for case $SRe_{\tau GL}^*$ (LL). Since these structures scale with semi-local wall units, their modulation is not related with outer layer motions.

Another way to quantify the turbulent structure is by means of pdfs. Figure 17 shows joint-pdfs of $\sqrt{\rho}u''/\sqrt{\tau_w}$ and $\sqrt{\rho}v''/\sqrt{\tau_w}$ as contour plots for the probability-weighted Reynolds shear stress
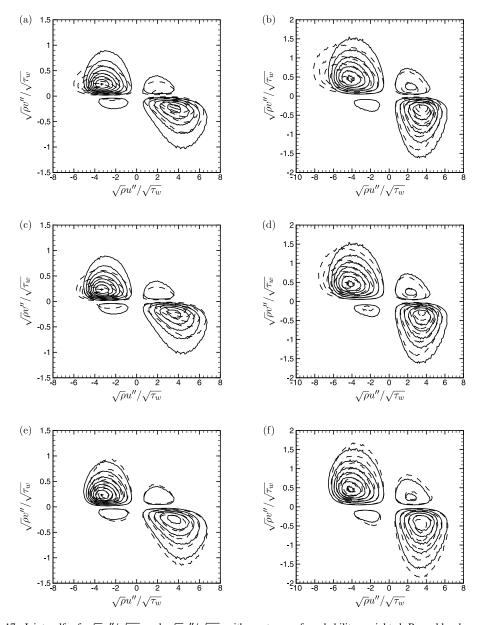

FIG. 17. Joint pdf of $\sqrt{\rho}u''/\sqrt{\tau_w}$ and $\sqrt{\rho}v''/\sqrt{\tau_w}$ with contours of probability weighted Reynolds shear stress $\rho u''v''/\tau_w P(\sqrt{\rho}u''/\sqrt{\tau_w}, \sqrt{\rho}v''/\sqrt{\tau_w})$, for (a) and (b) case GL, (c) and (d) case $SRe_{\tau GL}^*$, and (e) and (f) case LL, compared with CP395. Left column $y^* \approx 8.5$; right column $y^* \approx 15$. (——) Case CP395, (- - - -) case GL, $SRe_{\tau GL}^*$, LL.

$\rho u'' v'' / \tau_w P(\sqrt{\rho} u'' / \sqrt{\tau_w}, \sqrt{\rho} v'' / \sqrt{\tau_w})$ at $y^* \approx 8.5$ and $y^* \approx 15$. Since these plots are also affected by the preferential concentration of high density fluid in a low-speed streak, and vice versa, we use ρ instead of $\overline{\rho}$ for normalization. Each contour plot divides the probability-weighted Reynolds shear stress into four quadrants, according to the sign of u'' and v''. The most energetic events, which are responsible for generating the Reynolds shear stress, occur in quadrants Q2 and Q4 and are referred to as ejection ($u'' < 0$ and $v'' > 0$) and sweep ($u'' > 0$ and $v'' < 0$) events, respectively. The first observation that can be made from Figures 17(a), 17(c), and 17(e) is that in comparison to CP395, case LL (case GL and case $\mathrm{SRe}^*_{\tau GL}$) shows a larger (smaller) Reynolds shear stress as can be clearly seen from the spread of iso-contour lines. This is consistent with observations from Figure 11. An additional observation is related to the Reynolds shear stress generation mechanism. For case GL and $\mathrm{SRe}^*_{\tau GL}$, the pdfs in Q2 are clearly broader in stream-wise- and flatter in wall-normal direction. Thus, stronger negative stream-wise fluctuations and weaker positive wall-normal fluctuations appear. In other words, low-speed streaks are stabilised and do not lift as intensely for case GL and $\mathrm{SRe}^*_{\tau GL}$ ($Re^*_\tau \equiv \sqrt{(\overline{\rho}/\rho_w)}/(\overline{\mu}/\mu_w)Re_\tau$ decreases towards the channel center) when compared to CP395. The reverse happens for case LL (Re^*_τ increases) where low-speed streaks weaken and lift more intensely away from the wall.

V. CONCLUSION

Direct numerical simulations of a fully developed internally heated channel flow were performed under the low Mach number approximation. Six variable property cases with different relations for density and viscosity as a function of temperature were studied to analyse scaling of turbulent statistics and modulation of near-wall turbulence with respect to a constant property case. For all cases, the friction Reynolds number at wall was maintained constant with $Re_\tau = 395$.

Similar to constant property turbulent channel flows, where turbulent statistics can be expressed as a function of wall-normal distance y/h and friction Reynolds number Re_τ (based on wall quantities), we investigated if turbulent statistics for variable property turbulent flows can also be expressed as a function of y/h and semi-local Reynolds number Re^*_τ (based on semi-local quantities). First, a mathematical framework has been developed to support the use of the semi-local scaling hypothesis that has been initially proposed by Huang, Coleman, and Bradshaw[1] based on heuristic arguments. Then, the numerical simulations were used to test the semi-local scaling hypothesis by comparing turbulent statistics from different variable property turbulent flows. The validity of Morkovin's hypothesis that was used in the mathematical framework was assessed in the DNS database. The first comparison was done for a constant property case (CP395) with a case for which $\mu = \sqrt{\rho}$ (CRe$^*_\tau$), such that the semi-local scaling reduces to the classical wall scaling with $y^* = y^+$ and $Re^*_\tau = Re_\tau$ across the whole channel height. The comparison provided quasi-similar van Driest transformed stream-wise velocity profile $\overline{u}^{vd}$ and second order turbulent statistics, thus providing strong support for the validity of semi-local scaling. Two other comparisons (GL-SRe$^*_{\tau GL}$, Cν-SRe$^*_{\tau C\nu}$) involved variable property cases which exhibit quasi-similar Re^*_τ profiles, but different ρ and μ distributions across the channel. Both comparisons showed a good collapse of $\overline{u}^{vd}$ and second order turbulent statistics. All the above comparisons lead us to conclude that $\overline{u}^{vd}$ and second order turbulent statistics are a strong function of semi-local wall co-ordinates and their dependence on individual density or viscosity profile is minor. We further assessed the quasi-similarity of higher order statistics and found that the fourth order moments collapse reasonably well for all quasi-similar Re^*_τ cases, except GL-SRe$^*_{\tau GL}$ where small differences were seen due to high magnitudes of density fluctuation. The comparison of the third order moments, however, exhibited a breakdown of Morkovin's hypothesis, as they show a strong dependence on density fluctuations. A good collapse of third order moments among quasi-similar Re^*_τ cases was observed when $\sqrt{\rho} u''_i / \sqrt{\tau_w}$ was used as the fluctuating velocity scale.

Furthermore, the change in anisotropy of variable property turbulence has been quantified. For cases where $Re^*_\tau < Re_\tau$ in the channel core (GL and $\mathrm{SRe}^*_{\tau GL}$) the stream-wise Reynolds stress increased, while the wall-normal and span-wise Reynolds stresses decreased, causing an increase in near-wall stream-wise and span-wise anisotropy. The opposite is true for cases where $Re^*_\tau > Re_\tau$
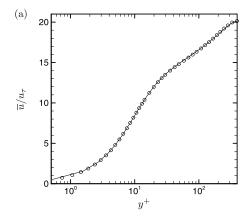
in the channel core (LL, Cν, and SRe$^*_{\tau C\nu}$). When compared with case CP395, the stream-wise anisotropy at $y^* = 0.5$ increased by 35% for case GL and SRe$^*_{\tau GL}$, while decreasing 20% for case LL and 13% for case Cν and SRe$^*_{\tau C\nu}$. This increased (decreased) anisotropy is not a Reynolds number effect, as highlighted by comparison with constant property turbulent flows at different Reynolds numbers form Iwamoto, Suzuki, and Kasagi.[32] The wall-normal anisotropy was independent of Reynolds number and property variations for all cases. A pre-multiplied 1D spectra was used to study the scaling of stream-wise Reynolds stress in the buffer layer for cases GL and LL at $y^* \approx 15$. The use of classical scaling (k_x^+, k_z^+) showed elongated (shortened) large-scale stream-wise structures with increased (decreased) mean span-wise spacing for case GL (LL). However, the stream-wise and span-wise non-dimensional length of the structures was found to be universal with respect to constant property cases when semi-local co-ordinates (k_x^*, k_z^*) were used. It was shown that an increase (decrease) in anisotropy for case GL (LL) is associated with strengthening (weakening) of large scale low-speed streaks in the buffer layer. Additionally, joint pdfs of stream-wise and wall-normal fluctuations revealed that the Reynolds shear stress generation was modified for cases where $Re_\tau^* \neq Re_\tau$ within the channel height. We showed that low-speed streaks are stabilised and do not lift as intensely for cases where Re_τ^* decreases towards the channel center. The reverse happens for cases where Re_τ^* increases towards the channel center, with low-speed streaks weakening and lifting more intensely away from the wall. The conclusions reported in the present work are general in nature and hence are applicable to any Newtonian fluid with heated or cooled wall as long as the basic assumptions made in the work hold.

ACKNOWLEDGMENTS

APPENDIX A: VALIDATION

The DNS code is validated with data from Moser, Kim, and Mansour,[2] Kim and Moin,[16] and Nicoud.[24] Figure 18 compares our result with data from Moser, Kim, and Mansour[2] for mean velocity and normal Reynolds stresses. Figure 19 shows similar comparison for budgets of turbulent kinetic energy and stream-wise Reynolds stress. As can be seen, all statistics show excellent agreement with Moser, Kim, and Mansour.[2] The scalar transport equation for the temperature has been validated with data extracted from Kim and Moin[16] for passive scalar simulations with $Re_\tau = 180$ and $Pr_w = 0.7$. The comparison of mean temperature and root mean square temperature fluctuation between present code and Kim and Moin[16] is given in Figure 20, again showing excellent agreement. The variable property influences are validated with data extracted from Nicoud,[24] who used
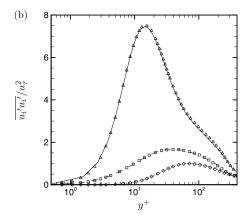

FIG. 18. (a) Mean velocity profile and (b) normal Reynolds stresses. Lines, case CP395; symbols, data from Moser, Kim, and Mansour.[2] In (b), (—, △) $\overline{u'u'}$; (······, ◇) $\overline{v'v'}$; (- - - -, □) $\overline{w'w'}$.
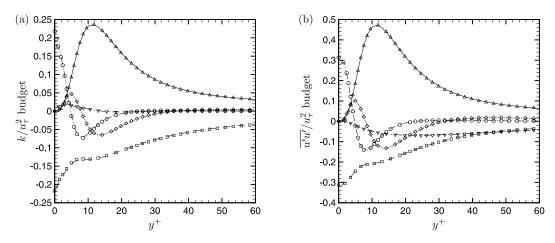
FIG. 19. (a) Turbulent kinetic energy $k = \overline{u_k' u_k'}/(2u_\tau^2)$ budget and (b) stream-wise Reynolds stress $\overline{u'u'}/u_\tau^2$ budget. Lines, case CP395; symbols, data from Moser, Kim, and Mansour.[2] (—, △) Production; (- - - -, □) dissipation; (······, ◇) turbulent diffusion; (— ·· —,○) viscous diffusion; (— · —,▽) turbulent pressure diffusion in (a) and pressure strain in (b).
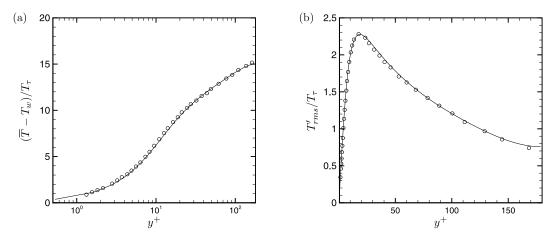

FIG. 20. (a) Mean temperature profile $(\overline{T} - T_w)/T_\tau$ and (b) root mean square of temperature fluctuations T'_{rms}/T_τ, T_τ is friction temperature defined as $T_\tau = q_w/(\rho c_p u_\tau)$. Lines, present code; symbols, data obtained from Kim and Moin.[16]
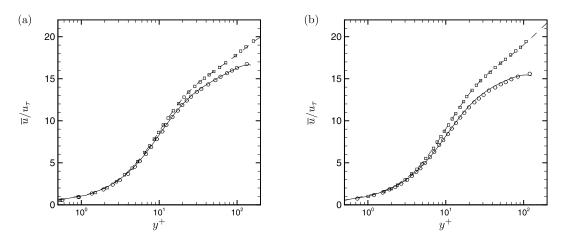

FIG. 21. Mean velocity profile for case with (a) $T_2/T_1 = 2$ and (b) $T_2/T_1 = 4$. Lines, present code; symbols, data obtained from Nicoud.[24] (—, ○) Hot side; (- - - -, □) cold side.

a low-Mach number solver to perform DNS of a turbulent channel flow between two isothermal walls with temperatures T_1 and T_2. The density, viscosity, and thermal conductivity are a function of temperature. Two cases corresponding to $T_2/T_1 = 2$ and $T_2/T_1 = 4$ are used for validation. The comparison of velocity profile on both hot and cold walls for two cases is shown in Figure 21. A reasonable collapse is obtained between present code and data from Nicoud.[24]

APPENDIX B: DERIVATION OF RE-SCALED MOMENTUM EQUATION FOR FLUCTUATING VELOCITY COMPONENTS

The momentum equations for the fluctuating components can be written as

$$\partial_{\hat{t}}(\hat{u}'_i) + \partial_{\hat{x}_j}(\hat{u}'_i\hat{u}'_j) + \partial_{\hat{x}_j}(\overline{\hat{u}_i}\hat{u}'_j) + \partial_{\hat{x}_j}(\hat{u}'_i\overline{\hat{u}}_j) \approx$$
$$-\partial_{\hat{x}_i}\hat{p}' + \partial_{\hat{x}_j}(\overline{\hat{u}'_i\hat{u}'_j}) + \partial_{\hat{x}_j}\left[\frac{1}{Re^*_\tau}\left(2\hat{S}'_{ij} - \hat{D}_{ij}\right)\right], \quad \text{(B1)}$$

where $\hat{S}'_{ij} = \frac{1}{2}\left(\partial_{\hat{x}_j}\hat{u}'_i + \partial_{\hat{x}_i}\hat{u}'_j\right) - \frac{1}{3}\partial_{\hat{x}_k}\hat{u}'_k\delta_{ij}$ and $\hat{D}_{ij} = \frac{\hat{u}'_i}{2}\left(\frac{\rho_w}{\overline{\rho}}\right)\partial_{\hat{x}_j}\left(\frac{\overline{\rho}}{\rho_w}\right) + \frac{\hat{u}'_j}{2}\left(\frac{\rho_w}{\overline{\rho}}\right)\partial_{\hat{x}_i}\left(\frac{\overline{\rho}}{\rho_w}\right) - \delta_{ij}\frac{\hat{v}'}{3}\left(\frac{\rho_w}{\overline{\rho}}\right)\partial_{\hat{y}}\left(\frac{\overline{\rho}}{\rho_w}\right)$. This equation can be further simplified by applying the product rule in the third and the fourth term,

$$\partial_{\hat{t}}(\hat{u}'_i) + \partial_{\hat{x}_j}(\hat{u}'_i\hat{u}'_j) + \overline{\hat{u}_i}\partial_{\hat{x}_j}(\hat{u}'_j) + \hat{u}'_j\partial_{\hat{x}_j}(\overline{\hat{u}_i}) + \hat{u}'_i\partial_{\hat{x}_j}(\overline{\hat{u}}_j) + \overline{\hat{u}}_j\partial_{\hat{x}_j}(\hat{u}'_i) \approx$$
$$-\partial_{\hat{x}_i}\hat{p}' + \partial_{\hat{x}_j}(\overline{\hat{u}'_i\hat{u}'_j}) + \partial_{\hat{x}_j}\left[\frac{1}{Re^*_\tau}\left(2\hat{S}'_{ij} - \hat{D}_{ij}\right)\right], \quad \text{(B2)}$$

and using continuity equations (16) and (21) the equation can be written for a fully periodic channel flow as

$$\partial_{\hat{t}}(\hat{u}'_i) + \partial_{\hat{x}_j}(\hat{u}'_i\hat{u}'_j) - \overline{\hat{u}_i}\frac{\hat{v}'}{2}\left(\frac{\rho_w}{\overline{\rho}}\right)\partial_{\hat{y}}\left(\frac{\overline{\rho}}{\rho_w}\right) + \hat{v}'\partial_{\hat{y}}(\overline{u})\delta_{i1} + \overline{\hat{u}}_j\partial_{\hat{x}_j}(\hat{u}'_i) \approx$$
$$-\partial_{\hat{x}_i}\hat{p}' + \partial_{\hat{x}_j}(\overline{\hat{u}'_i\hat{u}'_j}) + \partial_{\hat{x}_j}\left[\frac{1}{Re^*_\tau}\left(2\hat{S}'_{ij} - \hat{D}_{ij}\right)\right]. \quad \text{(B3)}$$

Replacing $\overline{\hat{u}}$ with $\sqrt{\frac{\overline{\rho}}{\rho_w}}\frac{\overline{u}}{u_\tau}$ using Equation (14), and applying the product rule we obtain

$$\partial_{\hat{t}}(\hat{u}'_i) + \partial_{\hat{x}_j}(\hat{u}'_i\hat{u}'_j) - \overline{\hat{u}_i}\frac{\hat{v}'}{2}\left(\frac{\rho_w}{\overline{\rho}}\right)\partial_{\hat{y}}\left(\frac{\overline{\rho}}{\rho_w}\right) + \hat{v}'\delta_{i1}\left(\sqrt{\frac{\overline{\rho}}{\rho_w}}\partial_{\hat{y}}\left(\frac{\overline{u}}{u_\tau}\right) + \frac{\overline{u}}{u_\tau}\partial_{\hat{y}}\left(\sqrt{\frac{\overline{\rho}}{\rho_w}}\right)\right)$$
$$+ \overline{\hat{u}}_j\partial_{\hat{x}_j}(\hat{u}'_i) \approx -\partial_{\hat{x}_i}\hat{p}' + \partial_{\hat{x}_j}(\overline{\hat{u}'_i\hat{u}'_j}) + \partial_{\hat{x}_j}\left[\frac{1}{Re^*_\tau}\left(2\hat{S}'_{ij} - \hat{D}_{ij}\right)\right]. \quad \text{(B4)}$$

$\partial_{\hat{y}}\left(\sqrt{\frac{\overline{\rho}}{\rho_w}}\right)$ can be expressed as $\frac{1}{2}\sqrt{\frac{\rho_w}{\overline{\rho}}}\partial_{\hat{y}}\left(\frac{\overline{\rho}}{\rho_w}\right)$, and using Equation (19) and (14) in the fourth and the fifth term, we get after algebraic manipulation the final form of the momentum equations

$$\partial_{\hat{t}}(\hat{u}'_i) + \partial_{\hat{x}_j}(\hat{u}'_i\hat{u}'_j) + \hat{v}'\partial_{\hat{y}}(\overline{u}^{vd})\delta_{i1} + \overline{\hat{u}}_j\partial_{\hat{x}_j}(\hat{u}'_i) \approx$$
$$-\partial_{\hat{x}_i}\hat{p}' + \partial_{\hat{x}_j}(\overline{\hat{u}'_i\hat{u}'_j}) + \partial_{\hat{x}_j}\left[\frac{1}{Re^*_\tau}\left(2\hat{S}'_{ij} - \hat{D}_{ij}\right)\right]. \quad \text{(B5)}$$

[1] P. G. Huang, G. N. Coleman, and P. Bradshaw, "Compressible turbulent channel flows: DNS results and modelling," J. Fluid Mech. **305**, 185–218 (1995).

[2] R. D. Moser, J. Kim, and N. N. Mansour, "Direct numerical simulation of turbulent channel flow up to Re = 590," Phys. Fluids **11**, 943–945 (1999).

[3] S. Hoyas and J. Jiménez, "Scaling of the velocity fluctuations in turbulent channels up to Re$_\tau$ = 2003," Phys. Fluids **18**, 011702 (2006).

[4] M. Bernardini, S. Pirozzoli, and P. Orlandi, "Velocity statistics in turbulent channel flow up to Reτ = 4000," J. Fluid Mech. **742**, 171–191 (2014).

[5] J. F. Morrison, B. J. McKeon, W. Jiang, and A. J. Smits, "Scaling of the streamwise velocity component in turbulent pipe flow," J. Fluid Mech. **508**, 99–131 (2004).

[6] N. Hutchins and I. Marusic, "Large-scale influences in near-wall turbulence," Philos. Trans. R. Soc., A **365**, 647–664 (2007).

[7] I. Marusic, R. Mathis, and N. Hutchins, "High Reynolds number effects in wall turbulence," Int. J. Heat Fluid Flow **31**, 418–428 (2010).

[8] I. Marusic, R. Mathis, and N. Hutchins, "Predictive model for wall-bounded turbulent flow," Science **329**, 193–196 (2010).

[9] A. J. Smits, "Turbulent boundary-layer structure in supersonic flow," Philos. Trans. R. Soc., A **336**, 81–93 (1991).

[10] G. N. Coleman, J. Kim, and R. D. Moser, "A numerical study of turbulent supersonic isothermal-wall channel flow," J. Fluid Mech. **305**, 159–183 (1995).

[11] L. Duan, I. Beekman, and M. P. Martin, "Direct numerical simulation of hypersonic turbulent boundary layers. Part 2. Effect of wall temperature," J. Fluid Mech. **655**, 419–445 (2010).

[12] M. Lagha, J. Kim, J. Eldredge, and X. Zhong, "A numerical study of compressible turbulent boundary layers," Phys. Fluids **23**, 015106 (2011).

[13] Y. Morinishi, S. Tamano, and K. Nakabayashi, "Direct numerical simulation of compressible turbulent channel flow between adiabatic and isothermal walls," J. Fluid Mech. **502**, 273–308 (2004).

[14] F. Nicoud and T. Poinsot, "Dns of a channel flow with variable properties," in *International Symposium on Turbulence and Shear Flow Phenomena (TSFP-1)* (Begell House, Santa Barbara, USA, 1999), pp. 697–702.

[15] H. Foysi, S. Sarkar, and R. Friedrich, "Compressibility effects and turbulence scalings in supersonic channel flow," J. Fluid Mech. **509**, 207–216 (2004).

[16] J. Kim and P. Moin, "Transport of passive scalars in a turbulent channel flow," in *Turbulent Shear Flows* (Springer, 1989), Vol. 6, pp. 85–96.

[17] R. Lechner, J. Sesterhenn, and R. Friedrich, "Turbulent supersonic channel flow," J. Turbul. **2**, 1–25 (2001).

[18] S. E. Guarini, R. D. Moser, K. Shariff, and A. Wray, "Direct numerical simulation of a supersonic turbulent boundary layer at mach 2.5," J. Fluid Mech. **414**, 1–33 (2000).

[19] T. Maeder, N. A. Adams, and L. Kleiser, "Direct simulation of turbulent supersonic boundary layers by an extended temporal approach," J. Fluid Mech. **429**, 187–216 (2001).

[20] S. Pirozzoli, F. Grasso, and T. Gatski, "Direct numerical simulation and analysis of a spatially evolving supersonic turbulent boundary layer at m= 2.25," Phys. Fluids **16**, 530–545 (2004).

[21] A. J. Smits and J.-P. Dussauge, *Turbulent Shear Layers in Supersonic Flow* (Springer Science & Business Media, 2006).

[22] A. Majda and J. Sethian, "The derivation and numerical solution of the equations for zero mach number combustion," Combust. Sci. Technol. **42**, 185–205 (1985).

[23] H. Nemati, A. Patel, B. J. Boersma, and R. Pecnik, "Mean statistics of a heated turbulent pipe flow at supercritical pressure," Int. J. Heat Mass Transfer **83**, 741–752 (2015).

[24] F. Nicoud, "Conservative high-order finite-difference schemes for low-mach number flows," J. Comput. Phys. **158**, 71–97 (2000).

[25] F. Zonta, C. Marchioli, and A. Soldati, "Modulation of turbulence in forced convection by temperature-dependent viscosity," J. Fluid Mech. **697**, 150–174 (2012).

[26] S. K. Lele, "Compact finite difference schemes with spectral-like resolution," J. Comput. Phys. **103**, 16–42 (1992).

[27] B. J. Boersma, "A 6th order staggered compact finite difference method for the incompressible Navier–Stokes and scalar transport equations," J. Comput. Phys. **230**, 4940–4954 (2011).

[28] Y. Morinishi, "Skew-symmetric form of convective terms and fully conservative finite difference schemes for variable density low-mach number flows," J. Comput. Phys. **229**, 276–300 (2010).

[29] P. A. McMurtry, W.-H. Jou, J. Riley, and R. Metcalfe, "Direct numerical simulations of a reacting mixing layer with chemical heat release," AIAA J. **24**, 962–970 (1986).

[30] P. Bradshaw, "Compressible turbulent shear layers," Annu. Rev. Fluid Mech. **9**, 33–52 (1977).

[31] H. Tennekes and J. L. Lumley, *A First Course in Turbulence* (MIT Press, 1972).

[32] K. Iwamoto, Y. Suzuki, and N. Kasagi, "Reynolds number effect on wall turbulence: Toward effective feedback control," Int. J. Heat Fluid Flow **23**, 678–689 (2002).